ACS Photonics

Article

Cite This: ACS Photonics XXXX, XXX, XXX−XXX

Sub-nanometer Thin Oxide Film Sensing with Localized Surface Phonon Polaritons

Rodrigo Berte,[†,‡,□] Christopher R. Gubbin,[§,□] Virginia D. Wheeler,[⊥] Alexander J. Giles,[⊥] Vincenzo Giannini,[†,∥] Stefan A. Maier,[†,¶] Simone De Liberato,[§] and Joshua D. Caldwell*[,⊥,#]

[†]The Blackett Laboratory, Department of Physics, Imperial College London, London SW7 2AZ, United Kingdom

[‡]CAPES Foundation, Ministry of Education of Brazil, Brasilia, DF 70040-020, Brazil

[§]School of Physics and Astronomy, University of Southampton, Southampton SO17 1BJ, United Kingdom

[⊥]U.S. Naval Research Laboratory, Washington, D.C., United States

[∥]Instituto de Estructura de la Materia (IEM-CSIC), Consejo Superior de Investigaciones Científicas, Serrano 121, 28006 Madrid, Spain

[¶]Nanoinstitut München, Fakultät für Physik, Ludwig-Maximilians-Universität München, 80799 München, Germany

[#]Department of Mechanical Engineering, Vanderbilt University, Nashville, Tennessee 37205, United States

Supporting Information

ABSTRACT: Chemical sensing methods based on surface polaritonic resonances stem from their intense near fields and resultant sensitivity to changes in local refractive index. Polar dielectric crystals (e.g., SiC, hBN) support surface phonon polaritons (SPhPs) from the mid-infrared to terahertz range with mode volumes and quality factors exceeding the best case scenario attained by plasmonic counterparts, making them strong candidates for resonant surface-enhanced infrared spectroscopy. We report on the behavior of SPhP resonances of SiC nanopillars following the incorporation of sub-nano- and nanometric coatings of Al_2O_3 and ZrO_2 obtained by atomic layer deposition. Concurrent anomalous red- and blue-shifts of SPhP resonances were observed upon deposition of sub-nanometric Al_2O_3 films, with shift direction dictated by the mode position relative to the ordinary longitudinal optic phonon of Al_2O_3. These concurrent shifts, which are attributed to coupling to the Berreman mode of the Al_2O_3 layer, persist for thicker films and are correctly predicted by numerical calculations employing the measured Al_2O_3 permittivity. Deposition of ZrO_2, whose phonon resonances are detuned from the SPhPs, also led to anomalous blue-shifts of transverse and longitudinal SPhP resonances around 900 cm^{-1} for films up to ∼1.5 nm, reversing to the canonical red-shift for thicker layers. These anomalous shifts were not reproduced numerically using the measured ZrO_2 permittivity and suggest the existence of a localized surface state, which when modeled as a simple Lorentz oscillator, provides semiquantitative agreement with experimental results. In addition, predicted shifts for thicker ZrO_2 layers may thus provide a tool for real-time monitoring of ultrathin film growth.

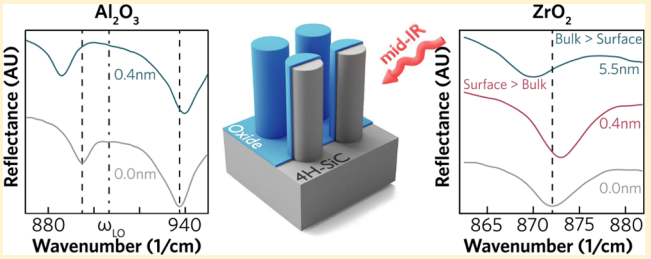

KEYWORDS: *surface phonon polaritons, oxides, atomic layer deposition, chemical sensing, ZrO_2, Al_2O_3*

In dielectric photonic systems, the interaction between nanoscopic quantum emitters and light is inherently weak as a result of the dimensional mismatch between diffraction-limited photonic modes and strongly localized emitters. This problem is traditionally overcome by exploitation of high-quality-factor optical microcavities, allowing photons to transit an emitter many times before escaping the system. Such tuning of the light−matter interaction allows for enhanced spontaneous emission via the Purcell effect[1] and, where the light−matter interaction rate exceeds the cavity line width, for a strong coupling regime with the formation of quasiparticles termed polaritons.[2]

An alternative way to achieve strong light−matter interactions is to circumvent the diffraction limit by transiently storing photonic energy in coherent oscillations of charges. In the case of an electronic charge, the resulting modes are termed plasmons.[3] In this case energy exists on an intermediate, morphologically dependent length scale, potentially orders of magnitude below that of the free-space photon. Increased spatial overlap between photons and emitters and the resulting near-field enhancements have yielded drastic efficiency improvements of naturally weak phenomena such as Raman scattering where single-molecule sensing has been achieved.[4] As the confinement is mediated by the electrons, tighter localization is always accompanied by increased ohmic losses,[5,6]

Received: December 5, 2017
Published: May 7, 2018

DOI: 10.1021/acsphotonics.7b01482
ACS Photonics XXXX, XXX, XXX−XXX

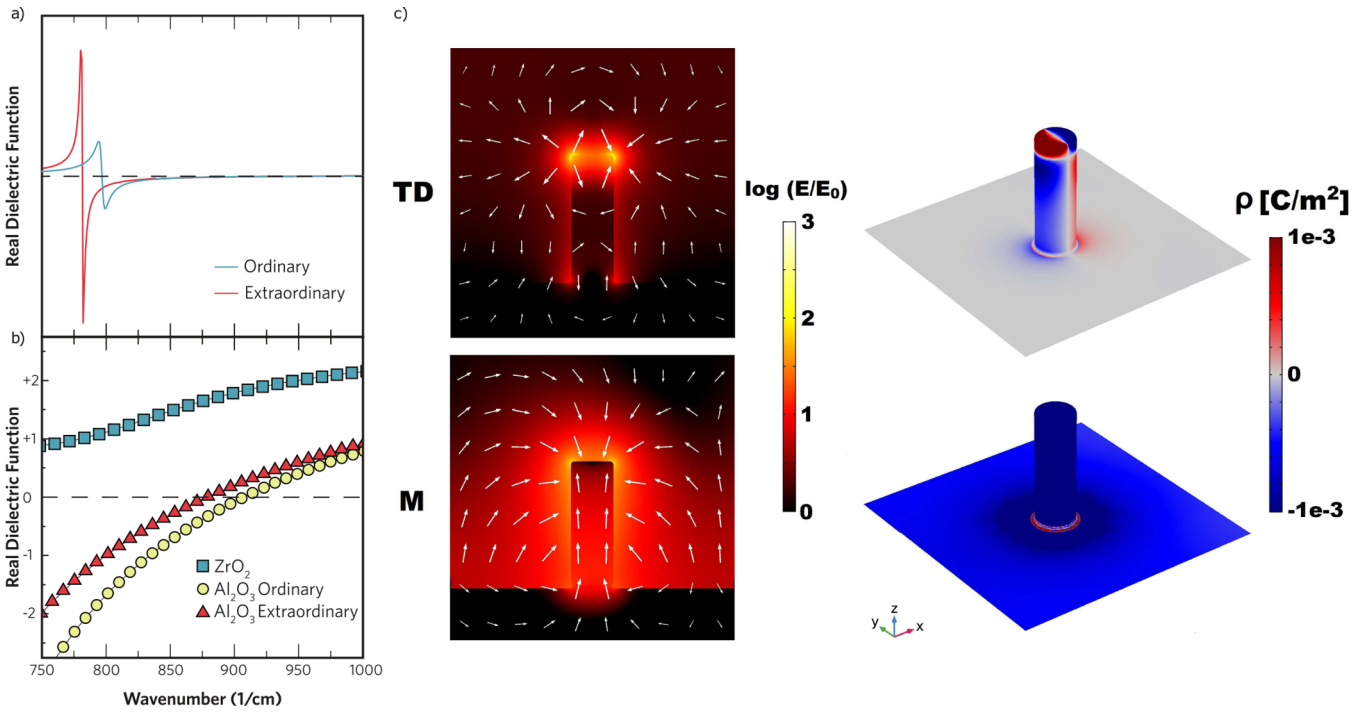

Figure 1. (a) Real component of the ordinary (blue) and extraordinary (red) dielectric function of 4H-SiC measured by ellipsometry. (b) Real component of the dielectric function of ZrO_2 (blue squares) and the ordinary (yellow circles) and extraordinary (red triangles) dielectric functions of Al_2O_3. (c) (Left) Cross-section of a nanopillar of diameter 300 nm, height 900 nm, and period 2000 nm showing the near-field (color scale) and electric field polarization (white arrows) of transverse dipolar (TD) and monopolar (M) modes. (Right) Respective surface charge density.

necessitating complex architectures to separate the field hotspot from the host metal[7] or incorporate external gain media.[8] An emergent alternative is surface phonon polaritons (SPhPs), modes formed by hybridization of free photons with coherent lattice oscillations of a polar dielectric crystal,[9] supported between the longitudinal (LO) and transverse (TO) optic phonon frequencies in a narrow, material and crystalline structure-dependent, spectral region called the Reststrahlen band. Like plasmons, these modes have characteristic lifetimes determined by that of their matter component; however, as optic phonons usually possess lifetimes 3 orders of magnitude longer than collective electron resonances in noble metals, SPhPs offer benefits commensurate with plasmons (e.g., subdiffractional confinement of light), while exhibiting significantly lower losses.

The morphologically dependent resonances supported by polar dielectrics[10−12] have been exploited for demonstration of extraordinary transmission,[13] subdiffraction imaging,[14] hyperlensing,[15,16] and surface-enhanced infrared absorption[17] and have been proposed as a platform for mid-infrared nonlinear optics.[18,19] In recent years tailored localized SPhP resonances with exceptionally narrow line widths were demonstrated in user-defined arrays of nanopillars on a substrate.[20,21] These narrow line widths permit the strong coupling of localized and propagating SPhPs, thereby allowing for predictive dispersion tuning.[22] In addition predictions of extreme near-field enhancements,[23] far exceeding the theoretical limit for plasmonic systems, would make such localized modes highly sensitive to very small changes in the local environment. Furthermore, the phonon-based nature of the SPhPs coupled with the strong surface sensitivity of the polaritonic near fields infers that small changes to the chemical bonding at the surfaces of SPhP nanostructures could have a large impact upon the resonant behavior.

While prior works have demonstrated that changing the local environment of a polaritonic nanostructure, such as the SiC nanopillars discussed here, results in a spectral red-shift of the resonance due to the increase in the effective local index of refraction of the ambient,[10,24] here we report on the observation of anomalous red- and blue-shifts in the localized SPhP resonances using ultrathin alumina (Al_2O_3) and zirconia (ZrO_2) coatings. These were obtained by atomic layer deposition (ALD), providing conformal, uniform thickness films on the surface of our nanopillars with strong, covalent bonding to the surface. We observed concurrent opposing blue- and red-shifts with the thinnest depositions of Al_2O_3, with shift direction dictated by the spectral position of the bare SPhP mode relative to the ordinary LO phonon of Al_2O_3, in the case of a blue-shift for modes localized at frequencies higher than the LO phonon and a red-shift for modes localized below it. The concurrent shifts persisted for thicker deposited films and are interpreted as a consequence of the coupling to the characteristic transverse mode observed near the LO frequency of thin dielectric films, named the Berreman mode.[25] This behavior is shown to be correctly reproduced by numerical simulations employing the measured permittivity of the deposited Al_2O_3 films. On the other hand, the deposition of ZrO_2 leads to blue-shifts of longitudinal and transverse SPhP resonances spectrally localized around 900 cm^{-1}. The anomalous shifts persisted for layers up to ~1.5 nm in thickness, reversing to the pure red-shift expected for a dielectric screening of resonances when the nanostructures were covered with thicker layers. This result cannot be explained by finite-element simulations utilizing the measured dielectric functions of the ZrO_2 films excluding diffractive

DOI: 10.1021/acsphotonics.7b01482
ACS Photonics XXXX, XXX, XXX−XXX

effects,[21,23] implying the influence of some microscopic process. To quantitatively explain the observed shifts, we introduce a localized surface state modeled as a Lorentz oscillator-permittivity which may represent a covalent bonding of the deposited film with the SiC surface, whose response dominates over the bulk optical response of the layer for sufficiently thin films. We demonstrate that such a theoretical model does indeed predict such reversible shifts when the pole of the surface state oscillator is spectrally located below the SPhP resonances of the SiC nanostructure. Such an approach results in interactions that can be interpreted as a consequence of strong coupling. With SPhPs being a strong candidate for resonant surface-enhanced infrared spectroscopy (SEIRA)-based sensing approaches, our results imply that ultrasensitive methods can be realized based on the strong surface sensitivity of the SPhP resonances with even small local changes to the ambient environment, with the magnitude of the anomalous spectral blue-shifts we report providing a key feature for distinguishing the thickness and potentially the chemical nature of the surface bond associated with the coating layer.

RESULTS

To determine the sensitivity of SPhPs to changes in the surface chemistry and local ambient, nanopillar arrays were fabricated from semi-insulating 4H-SiC substrates, using electron-beam lithography and reactive ion etching with details provided in the literature.[20,21] The Reststrahlen band of 4H-SiC lies between the transverse and longitudinal optic phonons. Due to the crystalline anistropy of 4H-SiC, there are actually two spectrally overlapping Reststrahlen bands due to the in- and out-of-plane phonons that occur between 797−969 and 784−964 cm^{-1}, respectively.[10] In this region the real component of the dielectric function, plotted in Figure 1a, is negative and nanopillars of the kind studied here support localized subdiffraction resonances. These narrow line width optical modes, separable into transverse dipole resonances with electric field orientated perpendicular and monopolar modes with electric field orientated parallel to the cylinder axis, demonstrate huge field enhancements at the resonator surface (Figure 1c).[20] In order to probe the modes' surface sensitivity, we employed Fourier transform infrared (FTIR) reflectance specroscopy of the SiC nanopillar arrays following iterative ALD of either Al_2O_3 or ZrO_2. This allowed for the spectral shift to be quantified as a function of the ALD coating thickness, while also providing overall trends. In addition, the choice of two distinct ALD materials offered the demonstration of the generality of the results.

Crystalline Al_2O_3 has six Reststrahlen bands in the mid-IR spectral range, each defined by a Coulomb-split pair of TO−LO phonons, with zeros in the permittivity at the LO frequencies.[26] The two highest energy bands are delimited by in- and out-of-plane LO modes at ∼906.6 and ∼881.1 cm^{-1}, respectively, both defininng positive values for the corresponding ordinary and extraordinary permittivities for frequencies higher than the LO modes themselves. Measurements of the permittivity of thin Al_2O_3 films grown on flat 4H-SiC substrates (Figure 1b) show good agreement with the reported values, even though ALD provides amorphous layers and the optical constants may not be invariant for ultrathin films (<5 nm).[27] Therefore, Al_2O_3 is not expected to provide the dielectric screening leading to a red-shift of localized SPhP modes following the oxide depositon.[24] However, upon deposition of a 0.35 nm thick layer of Al_2O_3, a red-shift of the monopolar (M) and a blue-shift of the transverse-dipolar (TD) mode were observed (bare resonances at 895 and 938 cm^{-1}, respectively, dashed lines in Figure 2b), as shown for a 300 nm diameter and

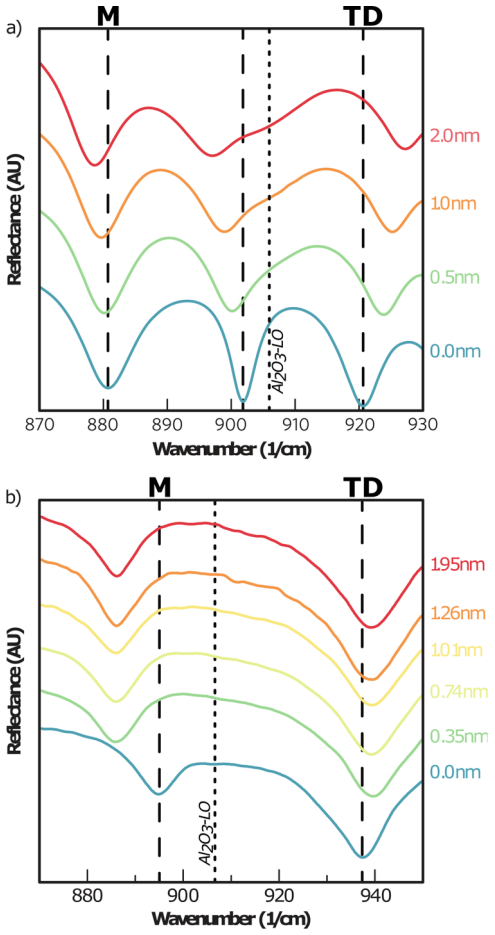

Figure 2. (a) Numerical reflectance of an array of 4H-SiC nanopillars of diameter 300 nm, height 900 nm, and period 700 nm. (b) Experimental reflectance of an array of 4H-SiC nanopillars of diameter 300 nm, height 900 nm, and period 700 nm. All are shown for varying Al_2O_3 overlay thicknesses.

700 nm period array, a behavior that persisted for thicker films. Notably, the ordinary LO phonon of the Al_2O_3 film lies between both resonances, shown as a vertical dotted line in Figure 2b. Numerically calculated reflectance of a pillar array of the same diameter and pitch incorporating the ordinary permittivity of Al_2O_3 as the ALD coating shows the same trend in monotonic shifts as the bare resonator modes (Figure 2a), with direction dependence on whether the bare mode lies above or below the ordinary Al_2O_3 LO phonon frequency at ∼906.6 cm^{-1} (vertical dotted line).[26] The additional resonance at ∼902 cm^{-1} observed in simulations corresponds to a longitudinal mode of the pillar, which, lying below the ordinary Al_2O_3 LO phonon, also red-shifts upon the film deposition. Experimentally this mode is merged with the TD mode, being spectrally resolved for larger pitches (see Supplementary Figure S2).

It is known that crystalline and amorphous thin films of dielectric materials exhibit sharp resonances in transmission/reflection of p-polarized light near their TO and LO phonons, the former due to TO modes being IR-active and the latter due to a phenomenon named the Berreman effect.[25,31] The

DOI: 10.1021/acsphotonics.7b01482
ACS Photonics XXXX, XXX, XXX−XXX

corresponding Berreman mode is a dispersive, leaky (wavevectors within the vacuum light cone) transverse mode in nature, excited by the normal compontent of the electric field relative to the film at frequencies slighly above the LO phonon of the material, where its positive dielectric function vanishes.[32] Although being able to propagate to the far field, the near-zero permittivity of the film allows this mode to provide huge subdiffractional confinement of the incident radiation. Thus, as a consequence of the extreme confinement of the resonator SPhP near the 4H-SiC surface, it is reasonable to interpret that the observed mode shifts occur due to their hybridization with the Berreman mode excited at frequencies slightly higher than the ordinary LO phonon of Al_2O_3.

Further evidence of the coupling to the Berreman mode is shown in Figure 3a, which illustrates the effect of a 0.35 nm

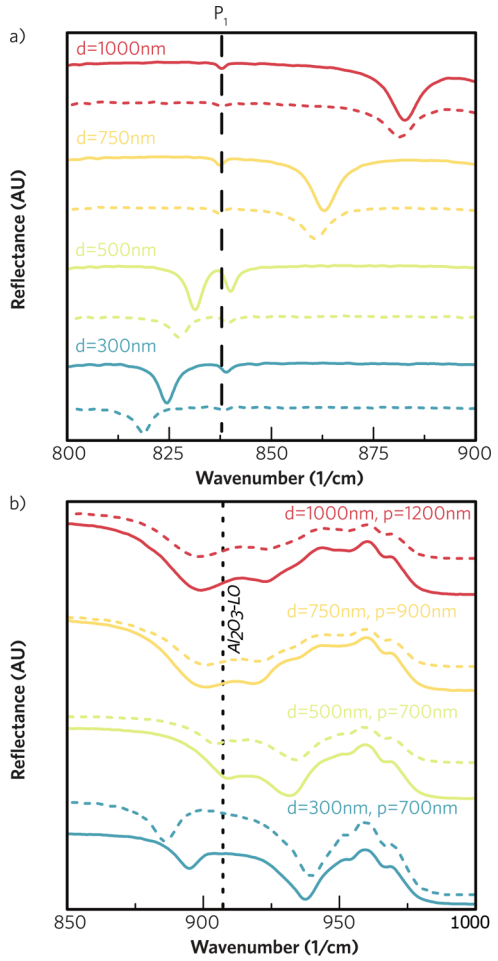

Figure 3. (a) Experimental reflectance from an array of 4H-SiC nanopillars of indicated diameter, height 900 nm, and period 2000 nm. (b) Experimental reflectance from an array of 4H-SiC nanopillars of the diameter and period indicated and height 900 nm. All are shown for the bare array (solid lines) and for a 0.35 nm Al_2O_3 coating (dashed). Ordinary LO phonon of Al_2O_3 shown as a vertical dotted line.

Al_2O_3 coating on the monopolar mode, which lies at lower frequencies than the Berreman mode, for a variety of nanopillar diameters. The bare reflectance is illustrated by the solid lines, and the coated by the dashed lines. In all cases deposition of an Al_2O_3 film results in red-shifted modal frequencies of the monopole. The larger shifts for smaller diameter pillars are a consequence of the reduced mode volumes and larger surface confinement provided by those.[23] Also noteworthy in these data is the strong coupling achieved between the resonator monopolar mode and the zone-folded LO phonon of the 4H-SiC substrate, near 837 cm^{-1} (P_1 mode, vertical dashed line in Figure 3a), an example of the hybridization observed between localized SPhP and modes of the patterned substrate,[28] which is also influenced by the shifts induced by the film deposition. The results for modes lying above and between the extraordinary and ordinary LO phonons of the film shown in Figure 3b are less clear, as the resonator arrays support many spectrally overlapping modes in this region. Nonetheless it is clear that modes lying below the ordinary LO phonon frequency at ~906.6 cm^{-1} (vertical dotted line in Figure 3b) red-shift, while those lying above blue-shift, inferring that the dominant hybridization is to the leaky mode near the ordinary LO phonon, again being more prominent for pillars of smaller diameter. Notably, the monopolar mode of the 500 nm diameter, 700 nm pitch resonator array, whose bare energy lies slightly above the LO phonon mode, also red-shifts. This might indicate a shifted epsilon-near-zero condition of the Berreman mode to higher frequencies due to a change in the effective permittivity of the thin film, induced by a chemical mechanism, by a substrate roughness comparable to the layer thickness, or even by a shift of the ordinary LO phonon due to mechanical stresses generated from the thermal expansion coefficient mismatch between Al_2O_3 and 4H-SiC.[29] However, due to the amorphous nature of ALD growth, the impact of stresses can be considered minimal. This should be considered in systems where epitaxial growth is included, for instance in thin films grown via molecular-beam epitaxy or chemical vapor deposition. It is important to note that the transverse, photonic modes of the resonator cannot directly hybridize with the longitudinal mode of the film in the absence of hydrodynamic effects, which are not included in our numerical simulations.[30] These further corroborate the hybridization between the SPhP and the leaky Berreman mode of the film, resulting from surface charges induced in the film by the out-of-plane component of the electric field provided by the localized modes.[25]

Contrasting with Al_2O_3, measurements of ZrO_2 films (>3 nm) deposited on a 4H-SiC substrate have shown that ZrO_2 has a relatively flat and uniformly ≥1 permittivity across the Reststrahlen band of 4H-SiC (illustrated by the blue squares in Figure 1b), which should provide a pure dielectric screening and shift to lower energies of all SPhP resonances upon thin film coating. However, contrary to prior work, following the deposition of ultrathin ZrO_2 films (5 cycles, 0.37 nm) an anomalous blue-shift is observed for SPhP resonances of both longitudinal and transverse-dipolar character near 900 cm^{-1}, as illustrated for different SiC nanopillar arrays in Figure 4b–d. With subsequent depositions, the resonances initially continue this anomalous shift; however, after 20 deposition cycles (~1.5 nm thick film) this shift is reversed and the anticipated red-shift is induced and continues with further film growth. For an array of nanopillars of diameter 300 nm and period 400 nm (Figure 4b), a monotonic red-shift is observed for the resonance at 873 cm^{-1}, while the anomalous reversible blue-shift is observed for the one at 900 cm^{-1}. The small periodicity for this array does not allow a unique assignment of a monopolar or transverse-dipolar character to these resonances, due to mode overlapping and hybridization at small gaps.[21] Figure 4c shows the anomalous behavior for both the monopolar (872 cm^{-1}) and the transverse-dipolar (905 cm^{-1}) resonances of a 300 nm

DOI: 10.1021/acsphotonics.7b01482
ACS Photonics XXXX, XXX, XXX−XXX

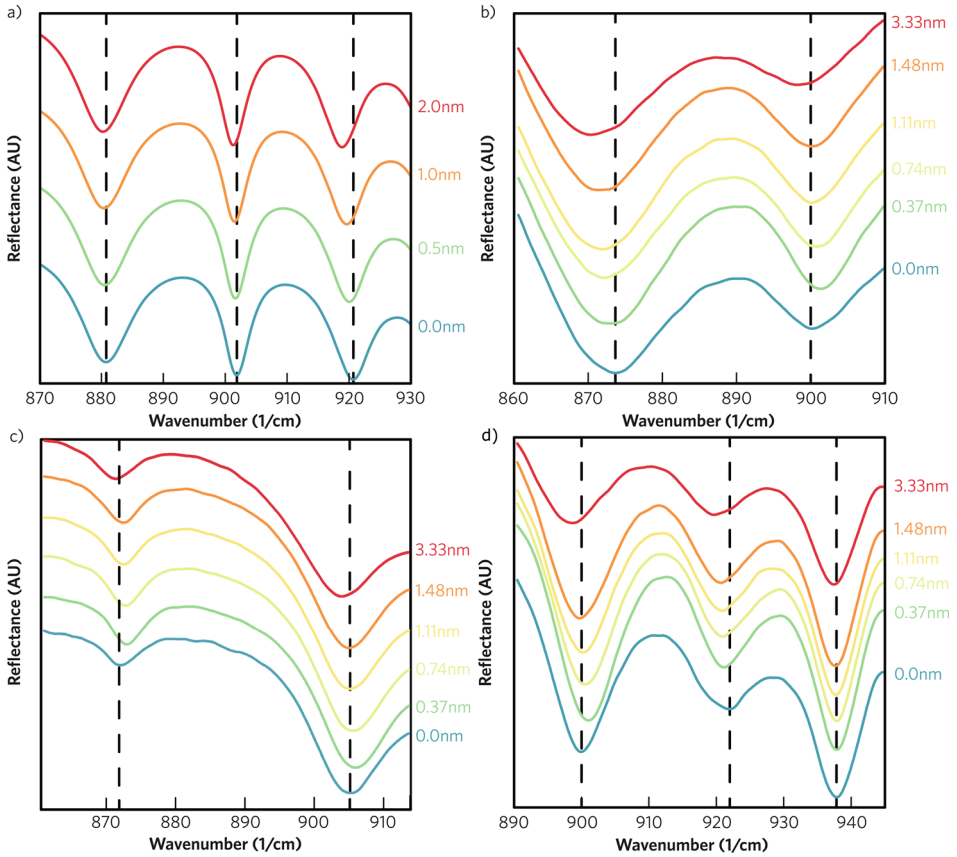

Figure 4. (a) Numerical reflectance of an array of 4H-SiC nanopillars of diameter 300 nm, height 900 nm, and period 700 nm. (b) Experimental reflectance of an array of 4H-SiC nanopillars of diameter 300 nm, height 900 nm, and period 400 nm. (c) Experimental reflectance of an array of 4H-SiC nanopillars of diameter 300 nm, height 900 nm, and period 700 nm. (d) Experimental reflectance of an array of 4H-SiC nanopillars of diameter 500 nm, height 900 nm, and period 1500 nm. All are shown for varying ZrO_2 overlay thicknesses.

diameter and 700 nm period array. Similar results are observed for an array of nanopillars of diameter 500 nm and array period 1500 nm, as shown in Figure 4d. Here monotonic red-shifts are observed for the modes with bare energies of 922 and 938 cm^{-1}, correspoding to higher-order transverse modes induced by corners and edges of the pillars,[28] as well as a reversible blue-shift seen for the lowest order transverse-dipolar mode with a bare energy of 900 cm^{-1}. This anomalous behavior was not reproduced by employing the measured permittivity of ZrO_2 films deposited on flat 4H-SiC substrates. This is illustrated in Figure 4a, which shows the numerically calculated reflectance of the same pillar array considered previously, whose three dominant modes red-shift monotonically as thicker coats of ZrO_2 are applied.

The shift of resonances with the thinnest ZrO_2 deposition layer was further investigated by exploring the tunability of localized SPhP with the array periodicity. The resultant spectral shifts for 300 nm diameter nanopillar arrays are plotted as a function of the original peak position of the uncoated structure in Figure 5a and for 500 nm diameter nanopillar arrays in Figure 5b. From this it is clear that regardless of the array geometry, anomalous shifts are spectrally localized around 900 cm^{-1}.

To eliminate the effect of altered diffractive coupling as a result of the presence of the ZrO_2 layer, the blue-shift of the transverse dipolar mode for a 0.37 nm thick coating was calculated for each lattice period and is shown as a function of gap size (equal to the array period minus the pillar diameter) in

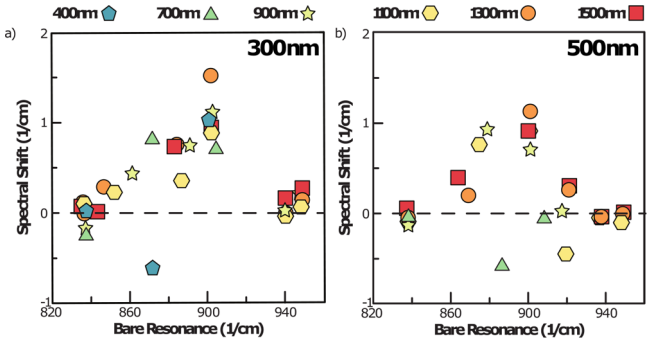

Figure 5. Relative shift as a function of original peak position for a 0.37 nm thick ZrO_2 layer deposited on arrays of nanopillars of (a) diameter 300 nm and height 900 nm; (b) diameter 500 nm and height 900 nm for varying array pitch.

Figure 6a. No clear dependence of the blue-shift upon the interpillar distance was observed, implying that the anomalous blue-shift is not mediated by near-field interaction between neighboring pillars and originates from some other mechanism. The magnitude and rate of shifts of the monopolar and transverse-dipolar modes of the 300 nm diameter and 700 nm period array as a function of Al_2O_3 and ZrO_2 thickness are shown in Figure 6b, corresponding to the spectra in Figure 2b and Figure 4c, respectively. A steady red-shift of both modes from the initial ~1 cm^{-1} blue-shift can be observed for thicker ZrO_2 deposited layers, while opposite shifts of larger magnitude, especially for the monopole, are obtained from

DOI: 10.1021/acsphotonics.7b01482
ACS Photonics XXXX, XXX, XXX−XXX

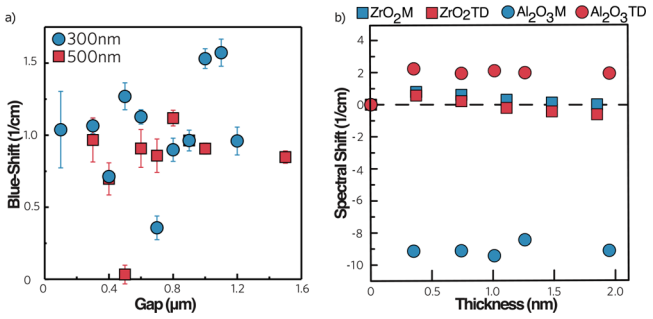

Figure 6. (a) Blue shift as a function of gap for nanopillars of diameter 300 nm (circles) and 500 nm (squares). (b) Relative shifts of the monopole (M) and transverse-dipole (TD) of the 300 nm diameter and 700 nm period pillar array as a function of the thickness of Al_2O_3 and ZrO_2 layers.

the initial Al_2O_3 deposition. Although the high reflectivity of Al_2O_3 within its Reststrahlen bands might prevent the accurate determination of peaks, the large initial shifts and the relative invariance with thicker layers might indicate that mechanisms other than the dielectric function of Al_2O_3 and the coupling to the Berreman mode may influence the shift behavior, such as the aforementioned coupling to longitudinal modes of the thin film. Nevertheless, the opposite trend relative to the ordinary LO phonon as qualitatively obtained with calculations is maintained for thicker films. To determine the role of the Zr precursor (zirconium(IV) *tert*-butoxide) utilized in the ALD process, additional spectra were recorded after five deposition cycles, but without incorporating the iterative exposure to the oxygen precursor, resulting in monotonic red-shifts. This resulted only in a small red-shift in the resonance frequencies (Supplementary Figure S1a,b). The potential of nonuniform pillar coverage or modified film morphology as the primary cause for the anomalous spectral shifts was also eliminitated, as control samples with zirconia layers of each of the same thicknesses were also grown in a single ALD deposition and provided quantitatively similar results to the those from the iterative depositions described above (Supplementary Figure S1c). This is further evidenced through atomic force microscopy (AFM) analysis of ZrO_2 films deposited on a 4H-SiC substrate, where conformal coating occurs even over substrate imperfections, leading to a smooth surface (RMS roughness <0.5 nm) for thicker ALD layers (Supplementary Figure S3).

DISCUSSION

The experimental data for Al_2O_3 qualitatively follows the results of our simple numerical calculations, utilizing the measured bulk-like dielectric function to describe the oxide film, even though its optical constants are expected to change for sub-nanometric thick layers.[27] The observed hybridization between the resonator modes and the leaky mode at frequencies of vanishing dielectric function near the ordinary LO phonons of the film presents a method to predictively tune the spectral landscape of a SPhP resonator system. In addition it demonstrates the potential of the strong near-field confinement of SPhP for sensing applications as large spectral shifts are observed for oxide film thicknesses of just 0.35 nm for which the sensitivity of macroscopic sensing methods such as ellipsometry is insufficient, especially for absorbing ultrathin films where a strong correlation between the film thickness and permittivity prevent their unique determination.[27]

The blue-shifts observed for ZrO_2, however, remain anomalous, not being explained by our simple model employing the measured permittivity of the 4H-SiC-deposited ZrO_2 and suggesting the influence of external effects. Studies on ultrathin SiO_2 films have shown the formation of a transition layer of different stoichiometry (SiO_x, $x \neq 2$), shape, and mechanical stress between the substrate and the deposited oxide, leading to an overall increase in the dielectric function in the visible range of the film when reducing its thickness,[33] a phenomenon that could lead to substantial deviations of the permittivity of sub-nanometric layers of ZrO_2 in the mid-IR. The presence of a native SiO_2 layer and its influence on the ALD growth of the Al_2O_3 and ZrO_2 films was evaluated experimentally through X-ray photoelectron spectroscopy (XPS) and also through numerical simulations (Supplementary Figure S4 and Figure S5). Although reported in the literature,[34] XPS analysis shows no indication of a native layer on the surface of the 4H-SiC. In addition, no mixing between the substrate with the ALD films is observed. Calculated effects of an eventual 1 nm SiO_2 layer show a pure red-shift of modes due to dielectric screening and also no alteration in the induced behavior by a second 0.5 nm cover layer of either ZrO_2 or Al_2O_3 (Supplementary Figure S5). Coordination defects in incomplete deposited layers could lead to a rearrangement of atoms in the structure of the thin film in the form of surface reconstructions, leading to properties different than displayed by the bulk material. This could influence the propagation of phonons in the underlying crystal and to shifts of the SPhP modes. However, the deposition of amorphous films through ALD and the random distribution of coordination defects in the layer are not expected to generate a well-defined reorganization of the film and to unidirectional SPhP mode shifting, an effect that could be more prominent if epitaxial growth techniques for crystalline layers were employed.[35] In addition, surface reconstructions in 4H-SiC would occur for temperatures above 900 °C, much higher than the 200 °C used here for ALD. Nevertheless, in order to explain experimental results, we introduce a process analogous to that observed for Al_2O_3, namely, hybridization with a spectrally interstitial resonance. The source of this resonance is assumed to be microscopic and localized to the interface between the 4H-SiC and the initial deposition of ZrO_2. Physically such a resonance could stem from either a vibrational bond between the 4H-SiC and either the ZrO_2 or residual precursor constituents,[36] a vanishing effective permittivity induced by surface roughness of the substrate leading to a leaky-mode coupling, or an interface dipole.[37] The elucidation of the nature of such surface state may be properly addressed by *ab initio* techniques and is outside the scope of this work. Regardless of its microscopic origin, the interstitial resonance can be effectively modeled by an additional homogeneous layer, characterized by the isotropic dielectric function

$$\epsilon(\omega) = \epsilon_\infty\left[1 + \frac{f\omega_0^2}{\omega_0^2 - \omega^2 + i\gamma\omega}\right] \quad (1)$$

where ϵ_∞ is the high-frequency dielectric constant, ω_0 is the transverse frequency of the proposed resonance, and f is the resonance oscillator strength.

To model the effect numerically, we consider a thin boundary layer of thickness 0.5 nm with resonant dielectric function of form eq 1 parametrized as $\epsilon_\infty = 2$, $f = 1.2$, $\omega_0 = 580$ cm^{-1}, $\gamma = 2$ cm^{-1}, whose longitudinal resonance therefore lies at

DOI: 10.1021/acsphotonics.7b01482
ACS Photonics XXXX, XXX, XXX−XXX

860 cm^{-1}, placed between the 4H-SiC resonator and the deposited ZrO_2 film, which are both described by their bulk dielectric functions. Numerical reflectance, for the same pillar array considered previously, is shown in Figure 7 for SPhP

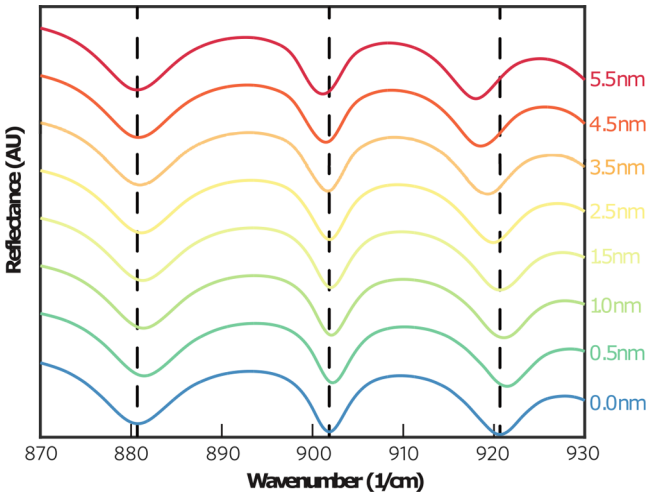

Figure 7. Numerical reflectance of a 300 nm diameter, 900 nm height, and 700 nm nanopillar array of 4H-SiC coated with a 0.5 nm layer of resonant dielectric parametrized by $\epsilon_\infty = 2, f = 1.2, \omega_0 = 580\ cm^{-1}, \gamma = 2\ cm^{-1}$ and a layer of ZrO_2. The total coating thickness is indicated.

resonances above the interstitial layer LO frequency, reproducing the blue-shifts of all modes after the first five deposition cycles as a result of coupling to the interstitial resonance, followed by weaker monotonic red-shifts as a result of the bulk ZrO_2 film. This denotes a transition in the overall optical response from the one dominated by anomalous shifts that can be interpreted as a strong coupling between the SPhP resonances with the LO resonance of the interstitial layer to the one where the dielectric screening provided by thick ZrO_2 overwhelms the interstitial layer effect. This behavior is consistent with that reported for the decreased interaction between interface phonons with thicker layers in heterostructures. A localized surface state stemming from a vibrational bond or an interface dipole might also be present in the case of Al_2O_3 deposition, but its effect may be overshadowed by the interaction with the Berreman and longitudinal modes of the thin film.

Finally we investigated the ability of full 3D finite-element method (FEM) calculations to predict spectral shifts as a function of the deposited film thickness. Raw spectra for selected peaks of nanopillars of diameter 500 nm and period 1300 nm are shown in Figure 8a. For thicker films the monotonic red-shifts predicted by numerical calculations are observed, allowing for comparison with experimental results. The squares in Figure 8b track the shifts of the higher-order pillar mode, whose bare frequency is indicated by the dashed line in Figure 8a as a function of film thickness. Circles indicate the corresponding numerical prediction. Both show a monotonic red-shift, and good agreement is reached considering the nominal fabrication values used for the geometry in numerical calculations. This given array period was chosen following a better correspondence observed by FEM predictions for larger pitches, where the pillar modes are spectrally separated.

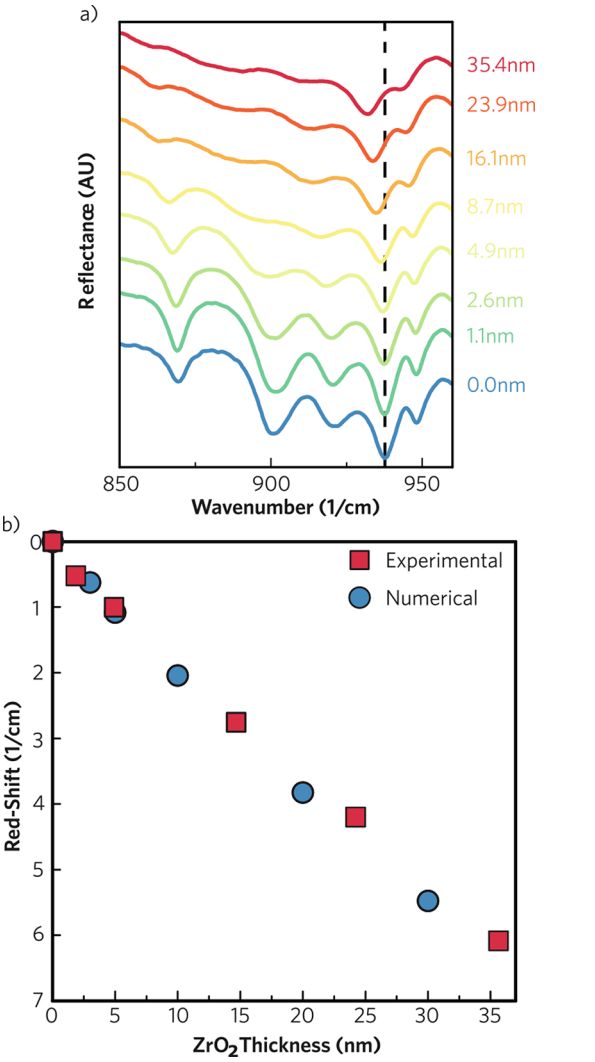

Figure 8. (a) Experimental reflectance from an array of 500 nm diameter nanopillars of 1300 nm period for the labeled thickness of ZrO_2 encapsulation. Dashed line indicates the bare frequency of the mode, whose shift is plotted as a function of ZrO_2 thickness as squares in (b). Circles indicate predictions from finite-element simulations.

CONCLUSIONS

In this paper we investigated the interaction of SPhPs supported by 4H-SiC nanopillar arrays with ultrathin oxide films deposited by ALD. The results for Al_2O_3 suggest hybridization between the tightly confined resonator modes and the leaky Berreman mode at frequencies slightly above the ordinary LO phonon of the oxide layer, in accordance with trends observed in numerical modeling results. For ZrO_2 films the anomalous spectral shifts observed for films of up to ~1.5 nm in thickness could not be explained by macroscopic electrodynamic calculations utilizing the measured dielectric function. The anomalous shifts may be explained as a result of hybridization of the SPhPs with a phenomenological phononic or electronic interface mode, which semiqualitatively reproduced the experimental results. Surface effects at the ZrO_2–air interface, such as dangling bonds from incomplete ALD reactions, leading to surface reconstructions of the thin film, could also be the cause of the observed anomalous shift, but are currently indistinguishable from the proposed interfacial mechanism. Thus, a deeper understanding of the phenomenon

DOI: 10.1021/acsphotonics.7b01482
ACS Photonics XXXX, XXX, XXX–XXX

necessitates the use of *ab initio* methods such as density functional theory. The strong spectral shifts observed, even for atomically thin films, demonstrate the potential of tightly confined SPhP modes for sensing applications. Moreover the predictable nature of the shifts for thicker films, which are in accordance with numerical expectations for thicknesses greater than 3 nm, may present an alternative for real-time thin film deposition monitoring. This work offers new prospects to the field of nanophotonics, exploring new light−matter interaction regimes of vibrational and optical modes and offering a new sensing platform in the mid-IR using low-loss plasmonic-like materials.

METHODS

Nanofabrication of SiC Nanopillar Arrays. Silicon carbide pillar arrays were etched into semi-insulating 4H-SiC substrates. Al/Cr hard masks defining the geometry of the pillar array were deposited on the substrate through electron-beam lithography, lift-off, and evaporation techniques. The pillar height was defined by the exposure time of a subsequent reactive ion etch, where the masked substrate was exposed for 38 min at 150 W utilizing SF_6 and Ar in equal partial pressures, followed by a chemical wet etch. In order to remove any residual fluorine, a commercial PlasmaSolv treatment was performed.

Atomic Layer Deposition. Conformal and highly uniform oxide film growth was performed in an Ultratech Savannah 200 reactor with a chamber temperature of 200 °C and a base pressure of 0.1 Torr prior to precursor injection. Sequential pulsing and purging of individual precursors was optimized to allow a homogeneous coverage of the high-aspect-ratio nanostructures. Zirconium(IV) *tert*-butoxide and trimethylaluminum were utilized as precursors for zirconia and alumina films, respectively, while deionized water acted as the oxygen source in both cases. Cation and oxygen precursors of oxide films were injected alternately in the ALD chamber, defining one deposition cycle and providing the self-limiting reactions leading to film growth. Linear growth rates were obtained for both oxides, with average deposition rates of 0.074 nm/cycle for ZrO_2 and 0.108 nm/cycle for Al_2O_3. To monitor the ALD process, a p-type Si witness sample was placed along the SiC in the reaction chamber for subsequent film thickness evaluation by ellipsometry.

Ellipsometry. Ellipsometry was employed to characterize the optical constants and thicknesses of deposited films. A J.A. Woollam alpha-SE spectrographic ellipsometer was utilized to collect the spectra across three different angles. Refractive index and film thickness were obtained by fitting the data with a Cauchy model. Film growth was obtained from measurements on the aforementioned Si witness sample. To reduce changes in optical properties due to lattice mismatch, oxide film spectra used for calculation were obtained from layers deposited over flat 4H-SiC substrates.

Fourier Transform Infrared Spectroscopy. Infrared measurements were performed in reflectance mode using a Thermo Scientific, Nicolet FTIR Continuum microscope. A 15×, 0.58 NA reverse Cassegrain objective provided illumination at angles of 10−35° off-normal, with a weighted average of 25°. Spectra were taken as an average of 32 scans with 0.5 cm^{-1} resolution acquired from a 50 μm^2 area.

Numerical Calculations. Frequency-domain, full-wave solutions of Maxwell's equations were obtained using the RF module of the finite-element solver Comsol Multiphysics. Plane-wave illumination was set at 25° (corresponding to the weighted-average illumination angle of the objective used in experiments) for a p-polarized incident field (transverse-magnetic mode). Bloch-periodic boundary conditions were applied to represent the periodicity of the arrays. Calculations were performed using the permittivities of 4H-SiC, ZrO_2, and Al_2O_3 as determined by ellipsometry.

ASSOCIATED CONTENT

Supporting Information

The Supporting Information is available free of charge on the ACS Publications website at DOI: 10.1021/acsphotonics.7b01482.

Reflectance spectra after zirconium precursor deposition in the absence of the oxygen precursor; reflectance spectra of iterative vs single-step growth of the ZrO_2 film; experimental and FEM calculations of spectra of 300 nm diameter pillar arrays of different pitches; AFM images and XPS analysis of ZrO_2 films deposited on flat 4H-SiC substrates; FEM calculations of effects of a 1 nm native SiO_2 layer on bare SiC modes and on Al_2O_3 and ZrO_2 deposition (PDF)

AUTHOR INFORMATION

Corresponding Author

*E-mail: josh.caldwell@vanderbilt.edu.

ORCID

Rodrigo Berte: 0000-0002-4171-2392
Christopher R. Gubbin: 0000-0003-3988-028X
Virginia D. Wheeler: 0000-0002-6024-9516
Joshua D. Caldwell: 0000-0003-0374-2168

Author Contributions

□R. Berte and C. R. Gubbin contributed equally to this work.

Notes

The authors declare no competing financial interest.

ACKNOWLEDGMENTS

R.B. acknowledges the Capes Foundation for a Science Without Borders fellowship (Bolsista da Capes, Proc. No. BEX 13.298/13-5). R.B. and S.A.M. acknowledge support from the Lee-Lucas Chair in Physics, the Office of Naval Research Global (Grant No. N62909-16-1-2027) and the Leverhulme Trust. S.D.L. is a Royal Society Research Fellow. S.D.L. and C.R.G. acknowledge support from EPSRC Grant No. EP/M003183/1. NRL coauthors acknowledge financial support from the Office of Naval Research administered by the Nanoscience Institute at the Naval Research Laboratory in Washington, D.C.

REFERENCES

(1) Gerard, J. M.; Sermage, B.; Gayral, B.; Legrand, B.; Costard, E.; Thierry-Mieg, V. Enhanced spontaneous emission by quantum boxes in a monolithic optical microcavity. *Phys. Rev. Lett.* **1998**, *81*, 1110−1113.

(2) Houdré, R.; Stanley, R. P.; Oesterle, U.; Ilegems, M.; Weisbuch, C. Room-temperature cavity polaritons in a semiconductor microcavity. *Phys. Rev. B: Condens. Matter Mater. Phys.* **1994**, *49*, 16761.

(3) Maier, S. A. *Plasmonics: Fundamentals and Applications*; Springer: New York, 2007.

(4) Kneipp, K.; Wang, Y.; Kneipp, H.; Perelman, L. T.; Itzkan, I.; Dasari, R.; Feld, M. S. Single molecule detection using surface-enhanced Raman scattering (SERS). *Phys. Rev. Lett.* **1997**, *78*, 1667−1670.

DOI: 10.1021/acsphotonics.7b01482
ACS Photonics XXXX, XXX, XXX−XXX

(5) Khurgin, J. How to deal with the loss in plasmonics and metamaterials. *Nat. Nanotechnol.* **2015**, *10*, 2−6.
(6) Khurgin, J.; Sun, G. Comparative analysis of spasers, vertical-cavity surface-emitting lasers and surface-plasmon-emitting diodes. *Nat. Photonics* **2014**, *8*, 468−473.
(7) Oulton, R. F.; Sorger, V.; Genov, D. A.; Pile, D. F. P.; Zhang, X. A hybrid plasmonic waveguide for subwavelength confinement and long-range propagation. *Nat. Photonics* **2008**, *2*, 496−500.
(8) Oulton, R. F. Plasmonics: Loss and gain. *Nat. Photonics* **2012**, *6*, 219−221.
(9) Caldwell, J. D.; Lindsay, L.; Giannini, V.; Vurgaftman, I.; Reinecke, T. L.; Maier, S. A.; Glembocki, O. J. Low-loss, infrared and terahertz nanophotonics using surface phonon polaritons. *Nanophotonics* **2015**, *4*, 44−68.
(10) Mutschke, H.; Andersen, A. C.; Clement, D.; Henning, T.; Peiter, G. Infrared properties of SiC particles. *Astron. Astrophys.* **1999**, *345*, 187−202.
(11) Caldwell, J. D.; Kretinin, A. V.; Chen, Y.; Giannini, V.; Fogler, M. M.; Francescato, Y.; Ellis, C. T.; Tischler, J. G.; Woods, C. R.; Giles, A. J.; Hong, M.; Watanabe, K.; Taniguchi, T.; Maier, S. A.; Novoselov, K. S. Sub-diffractional volume-confined polaritons in the natural hyperbolic material hexagonal boron nitride. *Nat. Commun.* **2014**, *5*, 5221.
(12) Dai, S.; Fei, Z.; Ma, Q.; Rodin, A. S.; Wagner, M.; McLeod, A. S.; Liu, M. K.; Gannett, W.; Regan, W.; Watanabe, K.; Taniguchi, T.; Thiemens, M.; Dominguez, G.; Neto, A. H. C.; Zettl, A.; Keilmann, F.; Jarillo-Herrero, P.; Fogler, M. M.; Basov, D. N. Tunable Phonon Polaritons in Atomically Thin van der Waals Crystals of Boron Nitride. *Science* **2014**, *343*, 1125−1129.
(13) Urzhumov, Y. A.; Korobkin, D.; Neuner, B.; Zorman, C.; Shvets, G. Optical properties of sub-wavelength hole arrays in SiC membranes. *J. Opt. A: Pure Appl. Opt.* **2007**, *9*, S322−S333.
(14) Taubner, T.; Korobkin, D.; Urzhumov, Y.; Shvets, G.; Hillenbrand, R. Near-field microscopy through a SiC superlens. *Science* **2006**, *313*, 1595−1595.
(15) Dai, S.; Ma, Q.; Andersen, T.; Mcleod, A. S.; Fei, Z.; Liu, M. K.; Wagner, M.; Watanabe, K.; Taniguchi, T.; Thiemens, M.; Keilmann, F.; Jarillo-Herrero, P.; Fogler, M. M.; Basov, D. N. Subdiffractional focusing and guiding of polaritonic rays in a natural hyperbolic material. *Nat. Commun.* **2015**, *6*, 6963.
(16) Li, P. N.; Lewin, M.; Kretinin, A. V.; Caldwell, J. D.; Novoselov, K. S.; Taniguchi, T.; Watanabe, K.; Gaussmann, F.; Taubner, T. Hyperbolic phonon-polaritons in boron nitride for near-field optical imaging and focusing. *Nat. Commun.* **2015**, *6*, 7507.
(17) Anderson, M. S. Enhanced infrared absorption with dielectric nanoparticles. *Appl. Phys. Lett.* **2003**, *83*, 2964−2966.
(18) Gubbin, C. R.; De Liberato, S. Theory of Nonlinear Polaritonics: $\chi^{(2)}$ Scattering on a β-SiC Surface. *ACS Photonics* **2017**, *4*, 1381−1388.
(19) Gubbin, C. R.; De Liberato, S. Theory of Four-Wave-Mixing in Phonon Polaritons. *ACS Photonics* **2018**, *5*, 284−288.
(20) Caldwell, J. D.; Glembocki, O. J.; Francescato, Y.; Sharac, N.; Giannini, V.; Bezares, F. J.; Long, J. P.; Owrutsky, J. C.; Vurgaftman, I.; Tischler, J. G.; Wheeler, V. D.; Bassim, N. D.; Shirey, L. M.; Kasica, R.; Maier, S. A. Low-Loss, Extreme Subdiffraction Photon Confinement via Silicon Carbide Localized Surface Phonon Polariton Resonators. *Nano Lett.* **2013**, *13*, 3690−3697.
(21) Chen, Y. G.; Francescato, Y.; Caldwell, J. D.; Giannini, V.; Mass, T. W. W.; Glembocki, O. J.; Bezares, F. J.; Taubner, T.; Kasica, R.; Hong, M. H.; Maier, S. A. Spectral Tuning of Localized Surface Phonon Polariton Resonators for Low-Loss Mid-IR Applications. *ACS Photonics* **2014**, *1*, 718−724.
(22) Gubbin, C. R.; Martini, F.; Politi, A.; Maier, S. A.; De Liberato, S. Strong and Coherent Coupling between Localized and Propagating Phonon Polaritons. *Phys. Rev. Lett.* **2016**, *116*, 246402.
(23) Gubbin, C. R.; Maier, S. A.; De Liberato, S. Theoretical investigation of phonon polaritons in SiC micropillar resonators. *Phys. Rev. B: Condens. Matter Mater. Phys.* **2017**, *95*, 035313.
(24) Bohren, C. F.; Huffman, D. R. *Absorption and Scattering of Light by Small Particles*; Wiley-VCH: Weinheim, 2004; pp 331−348.
(25) Harbecke, B.; Heinz, B.; Grosse, P. Optical Properties of Thin Films and the Berreman Effect. *Appl. Phys. A: Solids Surf.* **1985**, *38*, 263−267.
(26) Schubert, M.; Tiwald, T. E.; Herzinger, C. M. Infrared dielectric anisotropy and phonon modes of sapphire. *Phys. Rev. B: Condens. Matter Mater. Phys.* **2000**, *61*, 8187.
(27) Losurdo, M.; Bergmair, M.; Bruno, G.; Cattelan, D.; Cobet, C.; de Martino, A.; Fleischer, K.; Dohcevic-Mitrovic, Z.; Esser, N.; Galliet, M.; Gajic, R.; Hemzal, D.; Hingerl, K.; Humlicek, J.; Ossikovski, R.; Popovic, Z. V.; Saxl, O. Spectroscopic ellipsometry and polarimetry for materials and systems analysis at the nanometer scale: state-of-the-art, potential, and perspectives. *J. Nanopart. Res.* **2009**, *11*, 1521−1554.
(28) Ellis, C. T.; Tischler, J. G.; Glembocki, O. J.; Bezares, F. J.; Giles, A. J.; Kasica, R.; Shirey, L.; Owrutsky, J. C.; Chigrin, D. N.; Caldwell, J. D. Aspect-ratio driven evolution of high-order resonant modes and near-field distributions in localized surface phonon polariton nanostructures. *Sci. Rep.* **2016**, *6*, 32959.
(29) De Wolf, I. Micro-Raman spectroscopy to study local mechanical stress in silicon integrated circuits. *Semicond. Sci. Technol.* **1996**, *11*, 139−154.
(30) Roca, E.; Trallero-Giner, C.; Cardona, M. Polar optical vibrational modes in quantum dots. *Phys. Rev. B: Condens. Matter Mater. Phys.* **1994**, *49*, 13704.
(31) Vassant, S.; Hugonin, J. P.; Marquier, F.; Greffet, J. J. Berreman mode and epsilon near zero mode. *Opt. Express* **2012**, *20*, 23971−23977.
(32) Campione, S.; Brener, I.; Marquier, F. Theory of epsilon-near-zero modes in ultrathin films. *Phys. Rev. B: Condens. Matter Mater. Phys.* **2015**, *91*, 121408.
(33) Wang, Y.; Irene, E. A. Consistent refractive index parameters for ultrathin SiO_2 films. *J. Vac. Sci. Technol., B: Microelectron. Process. Phenom.* **2000**, *18*, 279−282.
(34) Huang, W.; Shao-Hui, C.; Xue-Chao, L.; Biao, S.; Tian-Yu, Z.; Xi, L.; Cheng-Feng, Y.; Yan-Qing, Z.; Jian-Hua, Y.; Er-Wei, S.; Wen-Hua, Z.; Jun-Fa, Z. Direct observation of nanoscale native oxide on 6H-SiC surface and its effect on the surface band bending. *Appl. Phys. Express* **2012**, *5*, 105802.
(35) Scopigno, T.; Steurer, W.; Yannopoulous, S. N.; Chrissanthopoulos, A.; Krisch, M.; Ruocco, G.; Wagner, T. Vibrational dynamics and surface structure of amorphous selenium. *Nat. Commun.* **2011**, *2*, 195.
(36) Caldwell, J. D.; Vurgaftman, I.; Tischler, J. G.; Glembocki, O. J.; Owrutsky, J. C.; Reinecke, T. L. Atomic-scale photonic hybrids for mid-infrared and terahertz nanophotonics. *Nat. Nanotechnol.* **2016**, *11*, 9−15.
(37) Butler, K. T.; Walsh, A. Ultra-thin oxide films for band engineering: design principles and numerical experiments. *Thin Solid Films* **2014**, *559*, 64−68.

DOI: 10.1021/acsphotonics.7b01482
ACS Photonics XXXX, XXX, XXX−XXX